applied sciences

MDPI

Article

LSTM-Based Autoencoder with Maximal Overlap Discrete Wavelet Transforms Using Lamb Wave for Anomaly Detection in Composites

Syed Haider Mehdi Rizvi [1], Muntazir Abbas [1,2,*], Syed Sajjad Haider Zaidi [1], Muhammad Tayyab [1] and Adil Malik [1]

[1] Department of Engineering Sciences, PN Engineering College, National University of Science and Technology, Karachi 75350, Pakistan; contacthaider.rizvi@gmail.com (S.H.M.R.); sajjadzaidi@pnec.nust.edu.pk (S.S.H.Z.); syed.tayyab@pnec.nust.edu.pk (M.T.); adil.malik@pnec.nust.edu.pk (A.M.)

[2] School of Water, Energy and Environment (SWEE), Cranfield University, College Road, Cranfield MK43 0AL, UK

* Correspondence: muntazir.abbas@pnec.nust.edu.pk

Abstract: Lamb-wave-based structural health monitoring is widely acknowledged as a reliable method for damage identification, classification, localization and quantification. However, due to the complexity of Lamb wave signals, especially after interacting with structural components and defects, interpreting these waves and extracting useful information about the structure's health is still a major challenge. Deep-learning-based strategy offers a great opportunity to address such challenges as the algorithm can operate directly on raw discrete time-domain signals. Unlike traditional methods, which often require careful feature engineering and preprocessing, deep learning can automatically extract relevant features from the raw data. This paper proposes an autoencoder based on a bidirectional long short-term memory network (Bi-LSTM) with maximal overlap discrete wavelet transform (MODWT). layer to detect the signal anomaly and determine the location of the damage in the composite structure. MODWT decomposes the signal into multiple levels of detail with different frequency resolution, capturing both temporal and spectral features simultaneously. Comparing with vanilla Bi-LSTM, this approach enables the model to greatly enhance its ability to detect and locate structural damage in structures, thereby increasing safety and efficiency.

Keywords: structural health monitoring; deep learning; Lamb waves; autoencoder; anomaly detection

Citation: Rizvi, S.H.M.; Abbas, M.; Zaidi, S.S.H.; Tayyab, M.; Malik, A. LSTM-Based Autoencoder with Maximal Overlap Discrete Wavelet Transforms Using Lamb Wave for Anomaly Detection in Composites. *Appl. Sci.* **2024**, *14*, 2925. https://doi.org/10.3390/app14072925

Academic Editor: Antonella D'Alessandro

Received: 11 June 2023
Revised: 31 July 2023
Accepted: 7 August 2023
Published: 30 March 2024

1. Introduction

Structural health monitoring (SHM) aims to evaluate large civil and mechanical infrastructures' structural integrity, reliability, and resilience [1,2]. The proper implementation of SHM ensures the functioning of these engineering structures by finding structural defects or irregularities before they cause catastrophic structural breakdown [3]. It involves measuring and evaluating the state properties of the underlying structure and relating these to define the performance parameter. Structural Health Monitoring (SHM) is an emerging field with immense industrial significance, incorporating innovative technology and evolving into a multidisciplinary area of research and development. Despite its growing importance, a recent study has yet to prove enough in many aspects. One primary concern is the reliability quantification of SHM systems, as current assessments primarily rely on visual inspections, which can be subjective and infrequent. On the other hand, existing data processing methods faced challenges from ambient noise, the volume of measurement data, the computation complexity, etc. [4]. These limitations hinder the widespread application of SHM across various industries [5].

The last decade has seen significant advances in machine learning, particularly in deep learning. Deep learning approaches are very effective in various tasks, yielding

cutting-edge outcomes across multiple engineering disciplines [6]. Recent advancement in artificial intelligence has also provided an opportunity to address these SHM challenges and elevate the capability and applicability of the SHM sector [7,8].

Recently, Rai and Mitra [9] proposed a 1D convolutional neural network (CNN) to detect damage in aluminium metallic structures. The proposed method can process raw signals and identify the different types of structural damage. Similarly, Wang et al. [10] presented a structural damage identification method based on integrating Hilbert–Huang transformation and CNN. Similarly, the author used a DNN with an autoencoder to compress the input data and a second neural network architecture to translate the compressed input into the damage characteristic. For guided wave (GW)-based fatigue crack diagnosis (FCD) on aluminium-alloy attachment lugs, Xu et al. [11] developed a CNN model. The trained multiclass CNN model predicted the crack length with an accuracy of 86.84%.

Similarly, Li et al. [12] employed a deep CNN network on a bridge. The author determined the deflection signal from the fibre-optic gyroscope sensor. The author exploited a data augmentation scheme to enhance the size of the datasets. The trained model generates an efficiency of 97% and outperforms many traditional machine learning algorithms. Many authors integrate multiple deep-learning networks. For example, ref. [13] combined 1D CNN and LSTM for acceleration data obtained from a three-story frame. The combined architecture decreases the computational cost, but the network is noise-sensitive.

Most of the damage detection strategies based on deep learning methods are mainly supervised and require data preprocessing and filtering methods to extract their key features. Moreover, most of the traditional deep learning methods require large amounts of training datasets, which is an expensive and time-consuming effort, requires expert knowledge, and hence generates a bottleneck in the automation system. Moreover, in SHM, there are other challenges associated with data collection and analysis such as high-dimensionality, data insufficiency, and class-imbalance. In a traditional ML approach, gathering a substantial and diverse dataset is crucial for accurately estimating the parameters of statistical models that describe all classes involved in efficient damage inspection [14]. However, in real situations, the collection of training data for all cases is often difficult, expensive, time-consuming, and resource intensive. In the literature [15–19], the viable solution for class imbalance or data insufficiency is data augmentation/enlargement. However, this approach becomes impractical when the training dataset lacks sufficient length to capture the fundamental discernible characteristics within the data. Additionally, any biases present in the original datasets will persist in the augmented dataset. Moreover, identifying an effective augmentation approach presents its own set of challenges.

In this paper, we trained a biLSTM-based autoencoder with maximal overlap discrete wavelet transform (MODWT) layer to accurately predict the signal anomaly and detect the presence of structural damage and, based on this, to help determine the damage location. MODWT decomposes the input signals into multiple levels of details with different frequency resolution which enables RNN to capture both temporal and spectral features simultaneously. This enhances the RNN capability to detect signal anomalies that exhibit specific time and frequency scale. The proposed scheme exploits only pristine/healthy signals and is trained without any labeling. So, the problem of supervised-based learning methods such as class imbalance and data insufficiency can be avoided. Once the proposed DL algorithm identifies the anomalous exciter-sensor path, damage localization can be done with the help of an image reconstruction algorithm. Figure 1 represents the flow chart of the proposed methodology used in this paper. The rest of the paper is organized as follows: in Section 2, a brief description of the autoencoder, LSTM, and MODWT layer is presented, while in the next section, the proposed methodology along with the experimental setup is explained. In Section 4, anomaly detection and damage localization based on the proposed methodology are performed, while the conclusion is drawn in the last section.

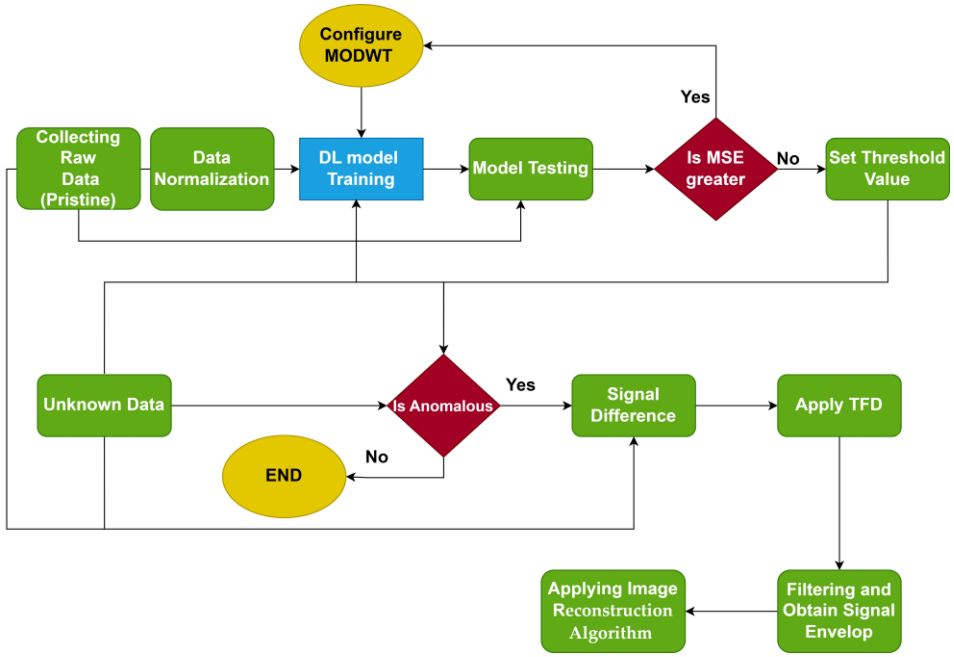

Figure 1. Flowchart for the proposed methodology.

2. Background

2.1. Autoencoder

Autoencoder, a particular type of deep learning network, is trained to replicate the input data. Anomaly detection, text generation, picture generation, image denoising, and digital communications are some areas where autoencoders outperform conventional engineering approaches in terms of accuracy and performance [20]. Autoencoder is an unsupervised learning traditionally consisting of two parts: encoder and decoder. The encoder compresses the data into a latent space vector, while the decoder tends to convert the latent space vector into the original input.

If the input to an autoencoder is a vector, $x \in \mathbb{R}^D$, then it will convert into another vector $z \in \mathbb{R}^D$ as

$$z = h(wx + b)$$

where h is a transfer function f the encoder, w is a weight matrix, and b is a bias vector. Then, the decoder converts an estimate of the original input vector, x, from the encoded representation, z, as follows:

$$x = h'(w'z + b')$$

where the quotation marks represent the other layer. The autoencoder learns to recognize and replicate the "standard" or "healthy" condition of the structural signals. When new data are introduced, the autoencoder tries to reconstruct them based on its understanding of the normal state. If the new data reflect an undamaged state, the autoencoder should accurately recreate them, resulting in a low reconstruction error. If the signal is damaged, containing ambiguous terms, then the autoencoder's attempts to rebuild the data using what it has learned from the undamaged pattern will result in a more significant reconstruction error [21].

2.2. RNN and BiLSTM

RNNs are a neural networks often employed for sequential data processing jobs. They are intended to deal with input data with temporal dependencies and where the sequence of the data points is essential. RNNs are excellent at applications, including speech recognition, natural language processing, and time series analysis [22]. The fundamental principle underlying RNNs is that they include feedback links that allow information to persist over time. This feedback mechanism allows the network to maintain memory and

capture long-term dependencies in the input [23]. Unlike feed-forward networks such as convolutional neural networks (CNNs), RNNs feature a recurrent connection where the last hidden state is an input to the next state; Figure 2 presents a typical RNN network.

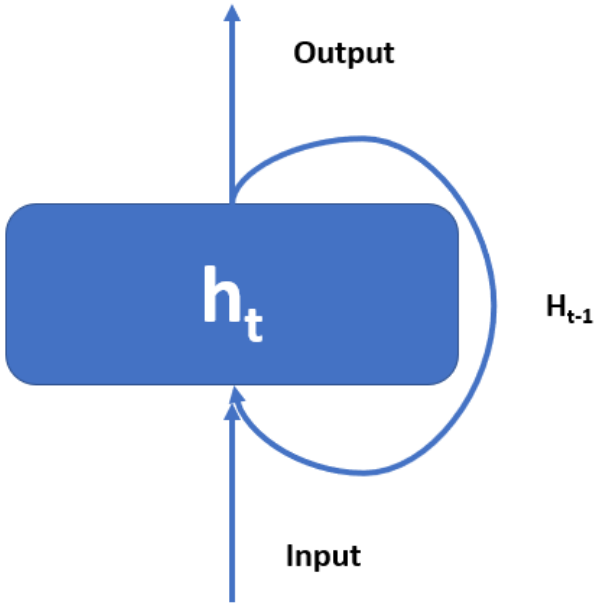

Figure 2. A typical RNN−based network.

LSTM layers are RNNs meant to learn and interpret long-term relationships in time-ordered data or sequences. Traditional RNNs frequently struggle to capture these long-term dependencies due to issues with "vanishing" or "exploding" gradients during training. The expressions "vanishing" and "exploding" gradients apply to circumstances in which the gradients become unexpectedly tiny or excessively big. These problems can impede the network's capacity to develop and sustain interactions over long periods. LSTM helps to address these challenges, improving its ability to grasp and recall information across extended periods. It handles gradient issues by incorporating additional gates that govern the flow of information within the hidden cell, determining what information is preserved for output and the next hidden state. With better control over information flow, LSTMs can more successfully learn and imitate long-term connections in data. LSTMs are more efficient than conventional neural networks such as ANN and CNN, which are less appropriate for collecting temporal correlations among sensor data [24].

A unit LSTM cell structure consists of three gates that control the flow of the data within the network as shown in Figure 3. The first is the forgetting gate (f_t) which eliminates the unnecessary data from the previous LSTM cell.

$$f_t = \sigma(W_f.[h_{t-1}, x_t] + b_f) \quad (1)$$

where σ denotes the sigmoid activation function while W represents the weight of forgetting gate. h_{t-1} and x_t are the output of previous LSTM cell and new input information, respectively. b_f shows the bias vector of the forgetting gate.

The input gate determines how much information should be carried for the current memory state based on the sigmoid function. On the other hand, the cell state is updated over time by incorporating new information through the input gate and selectively forgetting information through the forget gate. The process consists of two parts. First, sigmoid function is used to decide whether the new information should be updated or ignored while the other tanh function gives value to the information, representing its level of importance.

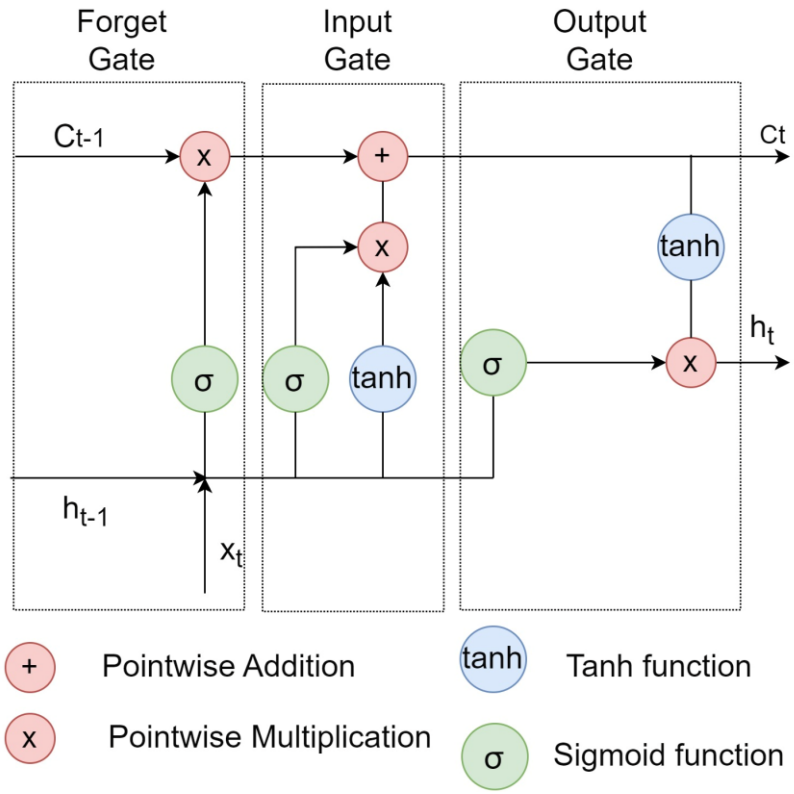

Figure 3. LSTM internal structure for a single unit.

$$i_t = \sigma(W_i.[h_{t-1}, x_t] + b_i) \tag{2}$$

$$C'_t = \tan h(\sigma(W_c.[h_{t-1}, x_t] + b_c)) \tag{3}$$

Now, the new cell is updated by multiplying f_t with the previous cell and then added to the new memory.

$$PC_t = C_{t-1} \times f_t + C'_t \times i_t \tag{4}$$

The output layer finally regulates the output produced by the LSTM at a specific time by the sigmoid activation function.

$$O_t = \sigma(W_o.[h_{t-1}, x_t] + b_o) \tag{5}$$

Th new hidden layer h_t is determined by

$$h_t = O_t \times \tan h(C_t) \tag{6}$$

On the other hand, the basic idea behind Bi-LSTMs is to have two independent LSTM layers, one processing the sequence ahead and the other processing it backwards. Each LSTM layer has its hidden state, and at each time step, the outputs of both layers are combined [25]. Figure 4 represents the general architecture of uniLSTM and biLSTM.

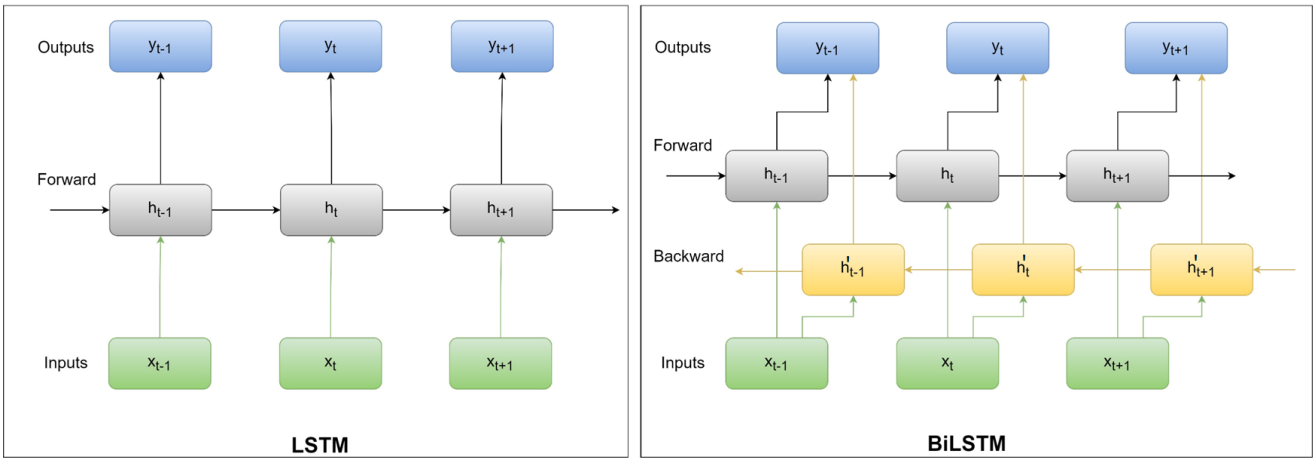

Figure 4. LSTM and biLSTM architecture.

2.3. Maximal Overlap Discrete Wavelet Transform

Multi-resolution analysis (MRA) is a signal processing technique used to analyze signals at multiple scales and resolution. The basic idea is convert the signal $x(t)$ into the number of successive approximations, each of which is the smoother version of $x(t)$ corresponding to a different resolution. MODWT is MRA that uses low- and high-pass filters to split the frequency spectrum of the input signal into scaling and wavelet coefficients. The traditional way of constructing the MODWT employs circular convolution directly in the time domain. However, the technique presented here performs the circular convolution within the Fourier domain, potentially improving processing efficiency and treating periodic signals [26].

To elaborate, the wavelet and scaling filter coefficients at a particular level, '*j*', are computed by first performing the signal's discrete Fourier transform (DFT) and the wavelet or scaling filter's DFT at the '*j*th' level. The DFT is a mathematical approach commonly used for frequency analysis of time-domain signals to transform a function of time into frequency. The product of these DFTs is then computed, which essentially captures the multiplication of their spectral components. This procedure relates to the time domain convolution of the original signals. Finally, the inverse DFT is done on this product which converts the information back into the time domain, producing the wavelet and scaling filter coefficients for the '*j*th' level [27].

This method efficiently computes the circular convolution in the Fourier domain before bringing it back into the time domain. The benefit of this approach is its computing efficiency and precision, which is especially useful for big datasets and when the signal or system of interest is intrinsically periodic or well-represented in the frequency domain.

Let H and G are jth level MODWT wavelet and scaling filters defined by orthogonal wavelets, respectively. If N represents the size of the sample which is an integer multiple of 2^j, then the DFT of the higher order wavelet filter is defined by

$$\frac{1}{N}\sum_{k=0}^{N-1} H_{j,k}e^{i2\pi k/N}, \qquad k = 0, \ldots\ldots, N-1 \tag{7}$$

$$H_{j,k} = H_{2^{j-1}k \bmod N}\prod_{m=0}^{j-2} G_{2^m k \bmod N}$$

where k is the width of the filter while $H_{j,k}$ is the jth level wavelet filter of the higher order. In addition, k mod N is k modulo N. Similarly, the jth level scaling filter is

$$\frac{1}{N}\sum_{k=0}^{N-1} G_{j,k}e^{i2\pi k/N} \tag{8}$$

where

$$G_{j,k} = \prod_{m=0}^{j-2} G_{2^m k \bmod N}$$

Figure 5 represents the MODWT of a Lamb wave signal. The original signal on the top is decomposed up to five decomposition levels with symlet wavelets. It captures both high and low frequency details and components, providing a comprehensive detailed of the signal.

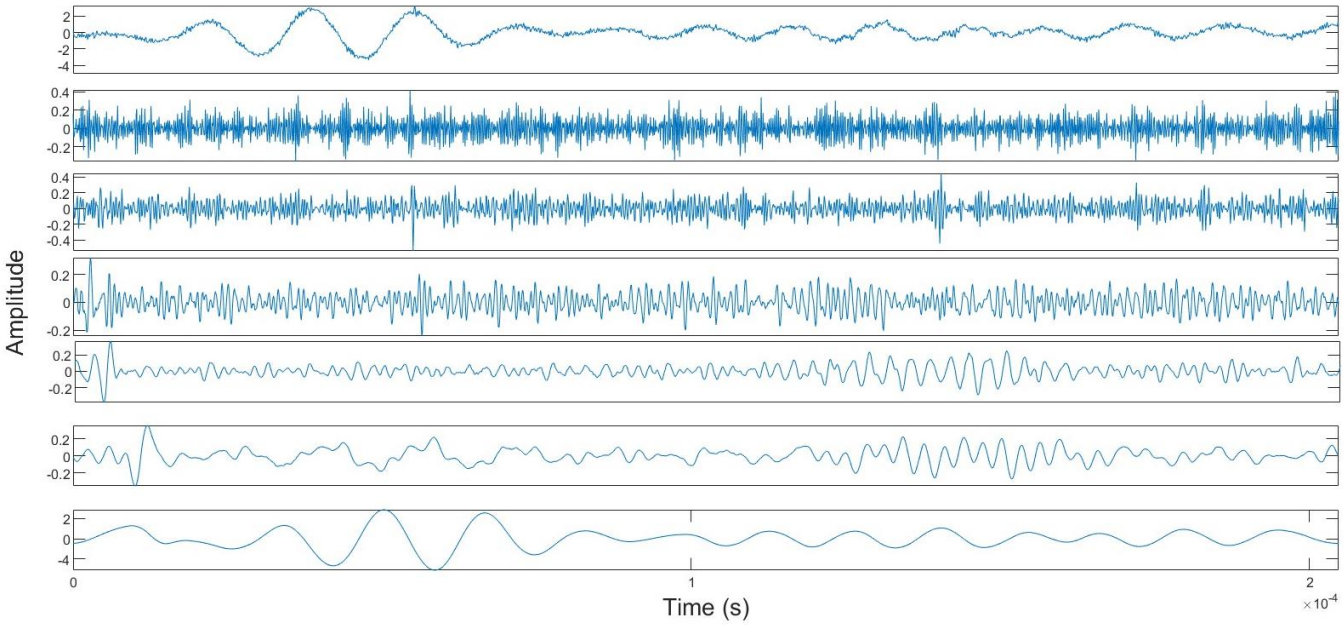

Figure 5. MODWT of damage Lamb wave signals.

3. Methodology

3.1. Experimental Datasets

In this paper, we utilize the datasets provided by the Open Guided Waves (OGW) platform [28]. Two carbon fibre plates having dimensions of 550 mm × 550 mm and a thickness of 2 mm are used. The thickness of each layer within the plates is 0.125 mm. Prepeg material Hexply M21/34%/UD134/T700/300, a particular kind of carbon fibre prepreg material from Hexcel®, is used for the plates. A quasi-isotropic (QI) layup pattern is used to organize the layers within the plates, which means that the layers are angled differently to offer balanced strength in various directions. The omega stringer, a separate component, is also composed of Hexply M21/34%/UD194/T700/IMA-12K carbon fibre prepreg material. The stringer features a [45/0/90/45/90/45]S quasi-isotropic layup pattern. The nominal thickness of the stringer is 1.5 mm, and each layer within the stringer has a thickness of 0.125 mm. The complete experimental setup is given in Figure 6a.

The plate has 12 piezoceramic transducers, surrounded by the stringer. These sensors are split evenly, with six on each side of the plate. Out of these sensors, six on one side act as actuators or exciters at a time, which are activated one by one, while the remaining 11 sensors receive the signals. So, each experiment collects a total of 66 separate signals from the decentralized and dispersed array of transducers' actuator-sensor pairs in a round-robin method, Figure 6b. The position of these transducers is given in Table 1.

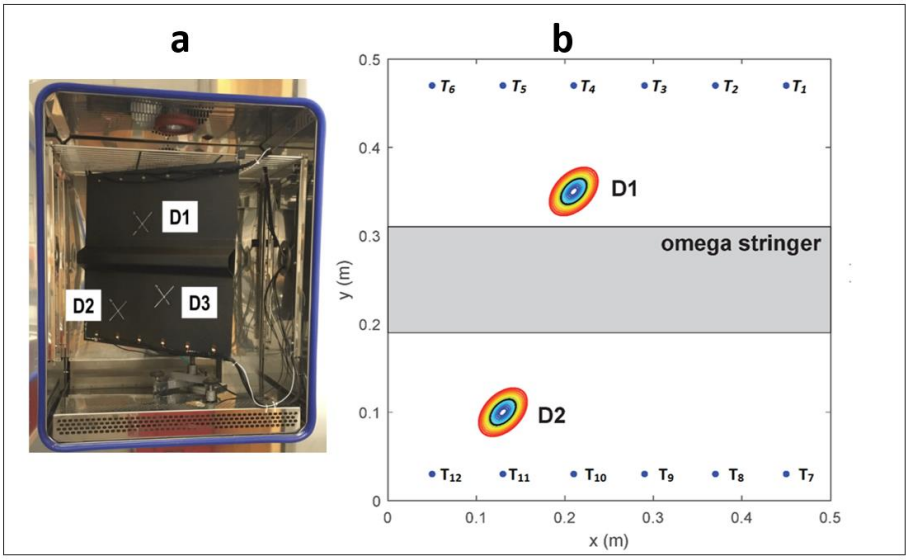

Figure 6. (**a**) Experimental Setup, (**b**) visualization of two damaged positions D1 and D2, and twelve transducers [28].

Table 1. Transducer/sensors position on pate.

Transducer/Sensor ID	Coordinates
1	(450, 470)
2	(370, 470)
3	(290, 470)
4	(210, 470)
5	(130, 470)
6	(50, 470)
7	(450, 30)
8	(370, 30)
9	(290, 30)
10	(210, 30)
11	(130, 30)
12	(50, 30)

For anomaly detection, we consider 60 kHz Lamb wave excitation frequency. A Hann-windowed five-cycle excitation pulse was generated. For the measurement, the author of [28] considered seven different phases. For phase 1, five measurements were recorded on the pristine structure. In phase two, reference defects were attached to the plate at position $D1$. An electromagnet with a metal block pressed the reference damage to the structure for maximum reliability. The electromagnet was then removed, leaving only the reference damage in contact with the structure. This process was repeated five times for each of the 13 damage sizes and positions. In the next phase, the author recorded another five baseline measurements after removing the reference damage. The author followed the same procedures for other damage positions in the next phases. Overall, 20 baseline and 520 damage measurements were recorded. Note that originally the author used three damage conditions present at different locations; however, in this study, we only considered two damage locations on the plate.

The stringer significantly impacts guided wave propagation, resulting in considerable signal changes. Here, the real challenge is used for raw signals and to extract useful information related to the state of the structure. To simplify the analysis, we focus only on the signals that traverse the plate and are received by sensors on the opposite side. As a result, out of the total 66 signals, we narrowed our attention to 36 signal paths. Moreover, we considered only 2048 sampling points as we were interested in the first-arriving waves and reflections from the damage and stringer. There are 720 datasets, of which 90% were

used for the training purpose while 10% were used for validation. Some of the waveforms are given in Figure 7.

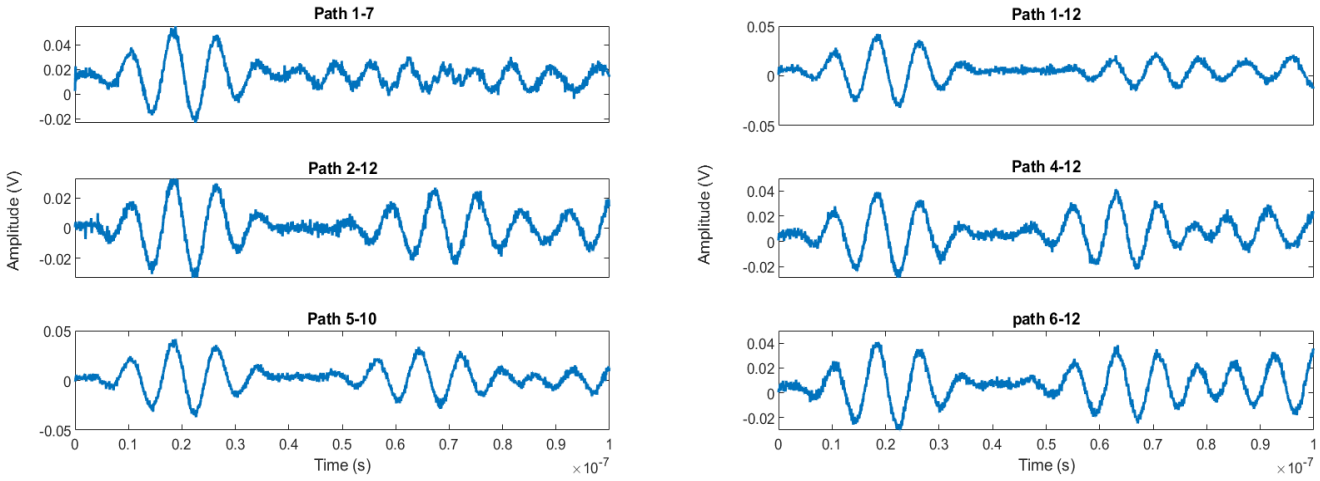

Figure 7. Waveform of few baseline signals at different exciter-sensor paths.

3.2. Model Training

In this study, we exploited three different autoencoders. The first is 1D CNN, in which the convolutional layer performs the function of a feature extractor. It employs appropriate filters or kernels to capture spatial and temporal interdependence in time-varying signals. To train the convolutional autoencoder, we built a hybrid model in which convolutional layers and BiLSTM were simultaneously used. The 1-D convolutional layer first filters the signal and removes the majority of the high-frequency noise. After that, the BiLSTM layer refines the signal features further. There is a total of 21 layers used with an overall 21,000 learnable. Figure 8 presents the architecture for the CNN network.

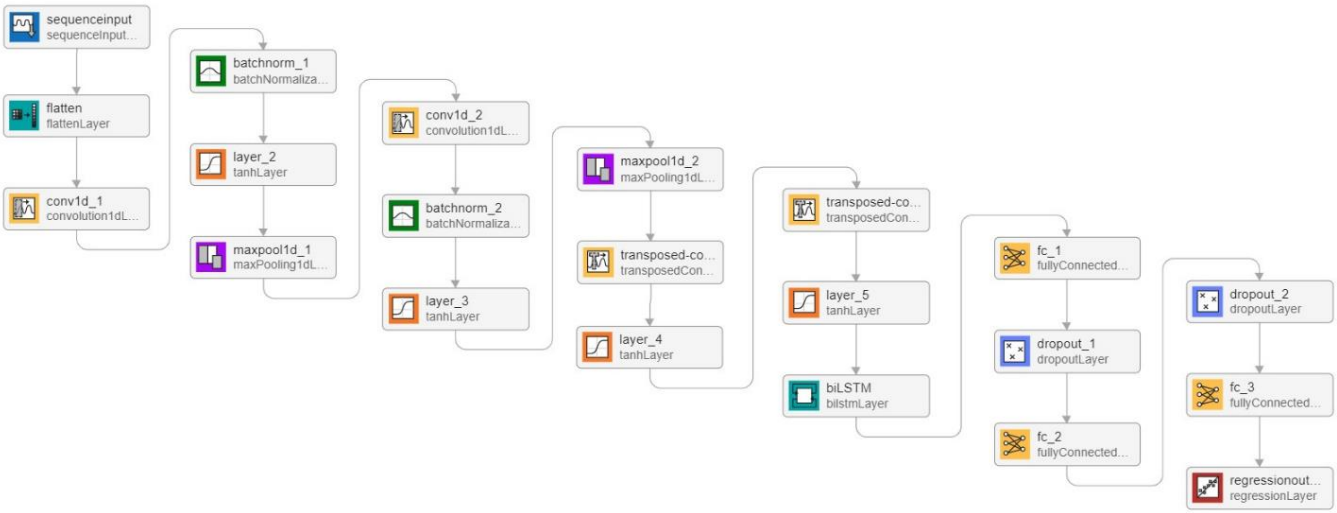

Figure 8. One-dimensional CNN architecture.

In the subsequent phase, a pure LSTM autoencoder model was developed. This model consisted of multiple bidirectional LSTM layers alternated with ReLU activation layers. These were later followed by a fully connected layer and a regression layer. There are nine layers in the model, with 29,300 learnable parameters. In the third phase, we added the MODWT layer with a multiresolution analysis algorithm in biLSTM architecture. This study used "Coiflets" orthogonal wavelets with five transform levels. The complete architecture is given in Figure 9 and all parameters are presented in Table 2.

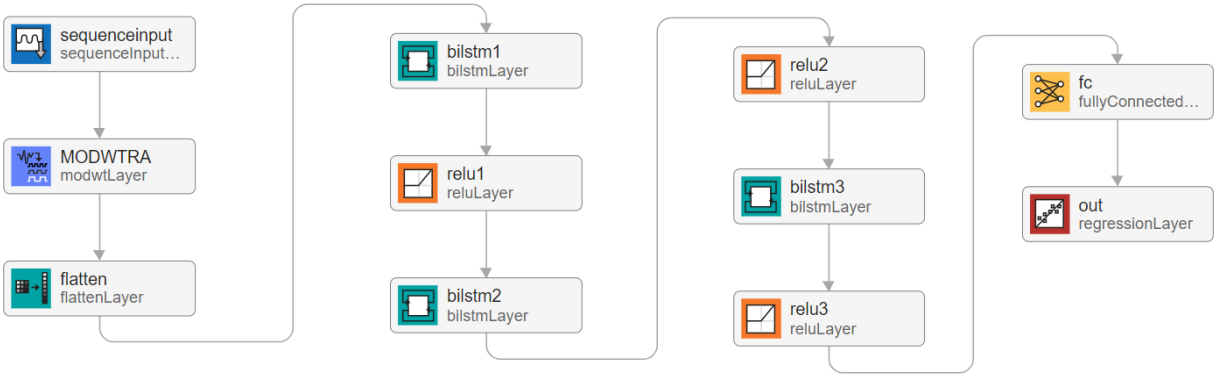

Figure 9. BiLSTM + MODWT layer autoencoder architecture.

Table 2. Proposed biLSTM + MOWDT layers.

	Layers	Learnable Properties	Number of Learnable
1	Sequence input		
2	MODWT	Weights 3 × 30	60
3	Flatten		
4	biLSTM 1 (32 hidden units)	Input weights = 128 × 5 Recurrent weights = 128 × 16 Bias = 128 × 1	2816
5	Relu 1		
6	biLSTM 2 (64 hidden units)	Input weights = 256 × 32 Recurrent weights = 256 × 32 Bias = 256 × 1	16,640
7	Relu 2		
8	biLSTM 3 (32 hidden units)	Input weights = 128 × 64 Recurrent weights = 128 × 16 Bias = 128 × 1	10,368
9	Relu 3		
10	Fully Connected	Weights = 1 × 32 Bias = 1 × 1	33
11	Regression Output		
		Total	29,900

Adam optimizer was used for training, which is suitable for nonstationary and nonlinear data such as Lamb wave signals, with a learning rate of 0.001. The minibatch size was 500, with a maximum epoch between 200 and 600, depending on the computational complexity. All the training was done using MATLAB® deep learning toolbox while all network architecture was designed and analyzed on the Deep network designer app provided by Mathwork®. Since 90% of baseline datasets are used for the model training, and 10% are used for validation purposes, the Table 3 represents the training and validation accuracy.

Table 3. Validation accuracy, RMSE and MAE of all three autoencoder architectures.

Deep-Learning Models	Accuracy	RMSE	MAE
1D CNN	81.44%	0.2347	0.1856
Bi-LSTM	84.75%	0.1950	0.1522
MODWT + Bi-LSTM	86.1%	0.1830	0.1439

As observed from the Table 3, when comparing with 1D CNN, it is evident that biLSTM performs better for the given datasets. However, adding the MODWT layer further enhanced the prediction accuracy of biLSTM and resulted in slightly lower RMSE

values. The model with biLSTM and MODWT layer can capture the signals' peak position, magnitude, and shape well.

Figure 10 shows the validation mean square error for all three architectures. Since there are 77 validations signals, we only present the first 30 signals here. It can be observed that the biLSTM with MODWT layer outperforms the other deep learning scheme and generates signals with better quality. Furthermore, Figure 11 shows the MAE for all exciter-sensor paths for all given datasets, determined by the proposed method.

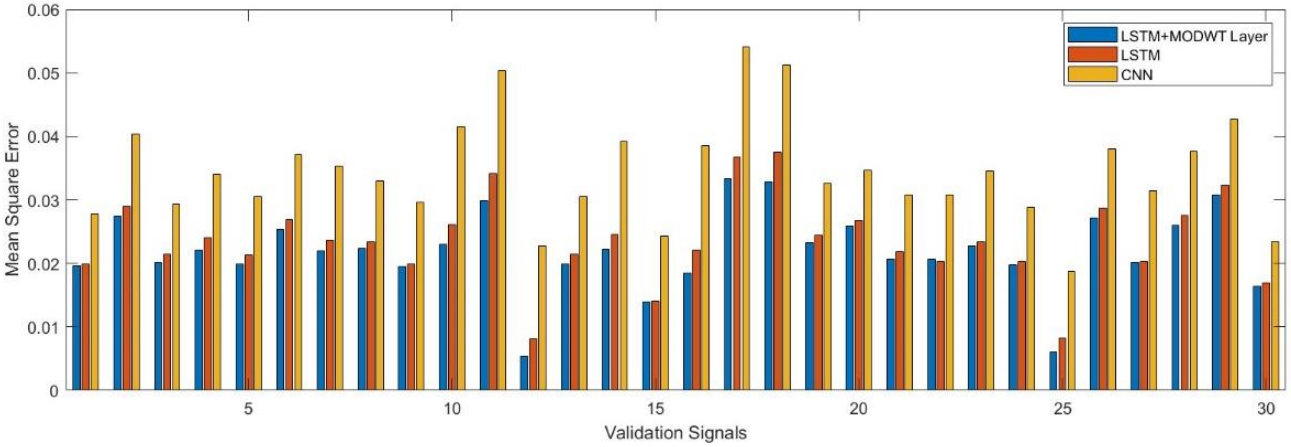

Figure 10. Validation errors for all three autoencoder architectures.

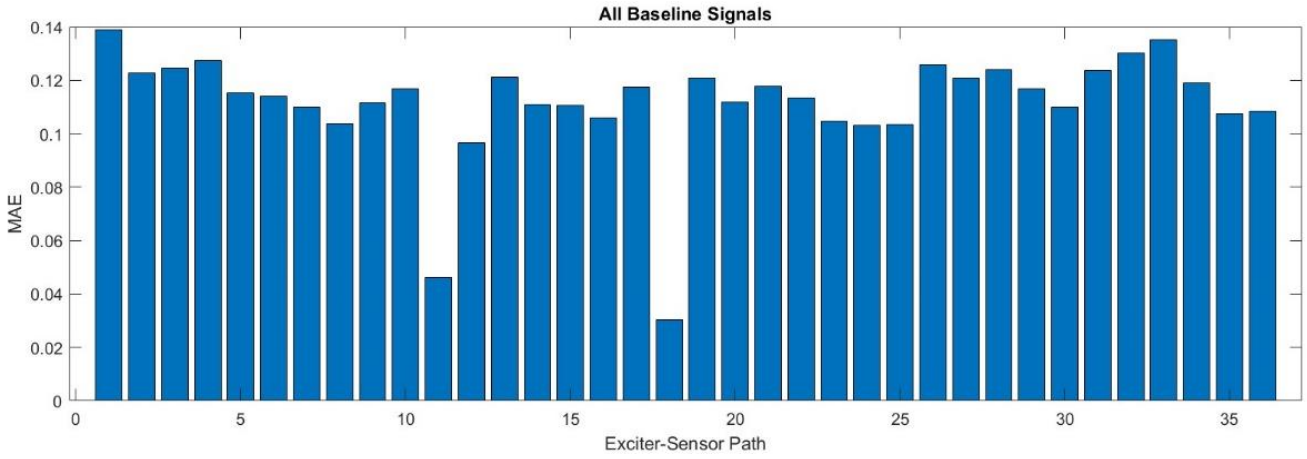

Figure 11. MAE for all datasets (training and validation) and divided into their respective excitor-sensor paths.

MODWT has a decomposition property that makes it suitable for analyzing both local and global features into different scales and levels. By analyzing signals at different levels, MODWT can identify the subtle variation in signals that may exist in different frequencies or time intervals. For example, we corrupted the original signals by adding noises of varied frequencies. Figure 12 shows that BiLSTM + MODWT detected anomalous behavior. This sensitivity allows for early detection and swift response.

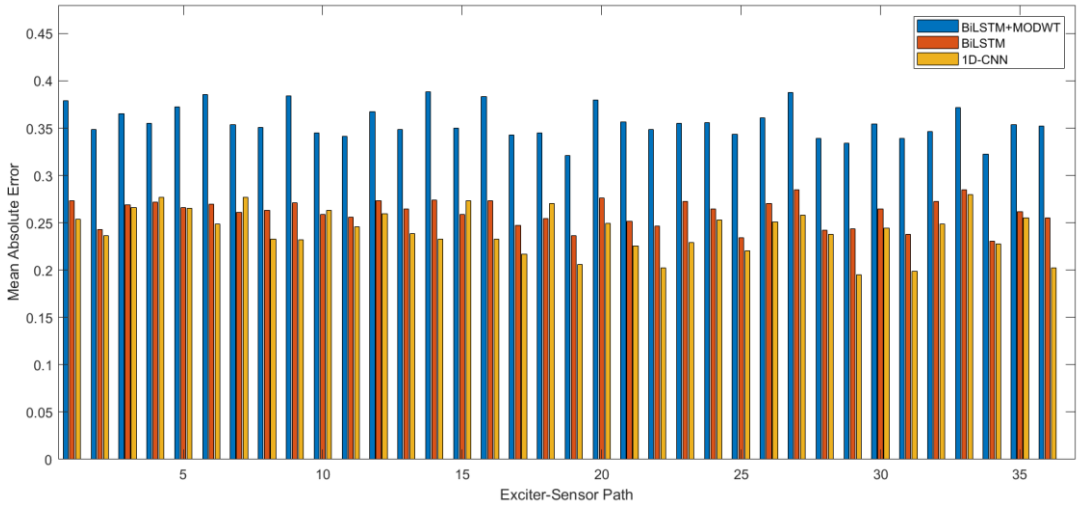

Figure 12. MAE for all three autoencoder architectures for subtle variations in signal.

4. Methodology

4.1. Anomaly Detection

An autoencoder-model-based anomaly detection system is usually trained solely on data corresponding to the pristine signal condition. As a result, the model is equipped to precisely reconstruct input that closely reflects inherent signal trends. Consequently, we can determine whether an input is an anomaly by examining its reconstruction error. The system classifies the input as an anomaly if the error surpasses a well-defined threshold. However, if the reconstruction error stays below this cutoff, the input is regarded as normal and consistent with typical normal signal patterns. The strength of this approach depends on the ability to identify unique signal variations. Since the model is trained only on pristine data, any significant deviation in the input, even one that does not align with known signal patterns, would lead to a higher reconstruction error. This means that the autoencoder can detect or flag anomalies as long as patterns deviate from the learned normal patterns. In this study, mean absolute error (*MAE*) was used to identify the signal anomaly which is determined by the Equation (9).

$$\widehat{MAE} = \frac{1}{N}\sum_{i=1}^{N}\left|\widehat{X_i} - \widehat{Y_i}\right| \tag{9}$$

where N is the size of the signals and $\hat{X}$ and $\hat{Y}$ correspond to the regenerated signals by the encoder for the original/pristine signal and the damage/received signal, respectively.

This study considers two damages placed at different locations, as shown in Table 4. For anomaly detection, we set the threshold value to be equal to 0.3, which was determined empirically by analyzing the baseline signals and validation data. Figure 13 presents the box plot for all three DL algorithms, explaining the statistical summary of the baseline data. We exploited maximum whisker value for determining the threshold values. Table 5 shows the threshold values for all DL algorithms.

Table 4. Damage Positions in specimen.

Damage ID	x-Coordinates (mm)	y-Coordinates (mm)
D1	210	350
D2	130	100

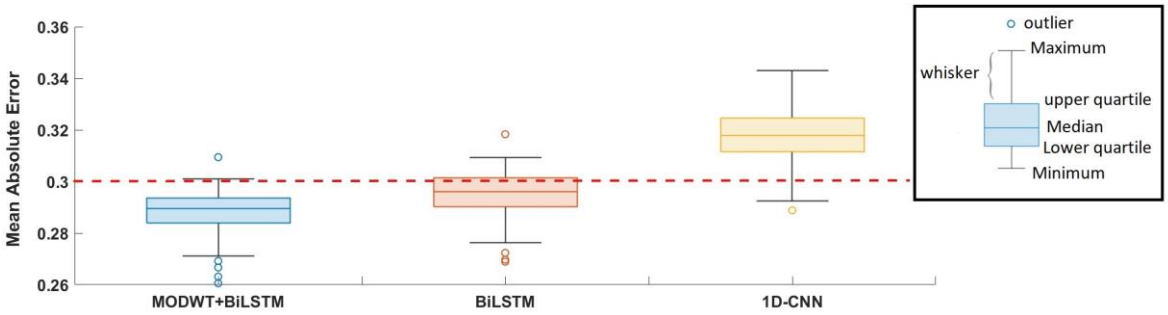

Figure 13. Box plot of all three deep-learning algorithms for determining threshold value.

Table 5. Threshold values for all three DL algorithms.

MODWT + RNN	RNN	1D-CNN
0.300	0.315	0.350

For damage identification D1, a total of 436 damage signals were extracted from the datasets, which were generated by conducting multiple experiments involving various damage sizes. Table 6 illustrates the results for true anomaly detection, false anomaly detection, and autoencoder accuracy. It was observed that the proposed method performed better than both biLSTM and 1D CNN methods. The MAE difference with the baseline signal obtained by the proposed scheme is shown in Figure 14. It can be observed that different bars surpassed the threshold value. Each bar represents a different pathway from the exciter sensor. Studying these bars, we can better understand which paths may pass through the damage. Similar to identifying anomalous signals, this visualization aids in detecting irregularities or deviations that might signify damage in specific paths. Similarly, Figure 15 shows error values for D2 which show significant deviations from the learner learned pattern. Peaks are also observed in both figures generated when the exciter-sensor path directly passes or is close to the damage. Table 7 shows the average *MAE* values for D1 and D2.

Table 6. All three autoencoder accuracy in detecting damage signal (D1).

Deep Learning Models	True Anomaly Detection	False/Missed Detection	Accuracy
MODWT + BiLSTM	385	51	88.3%
BiLSTM	375	61	86.0%
1D-CNN	351	85	80.5%

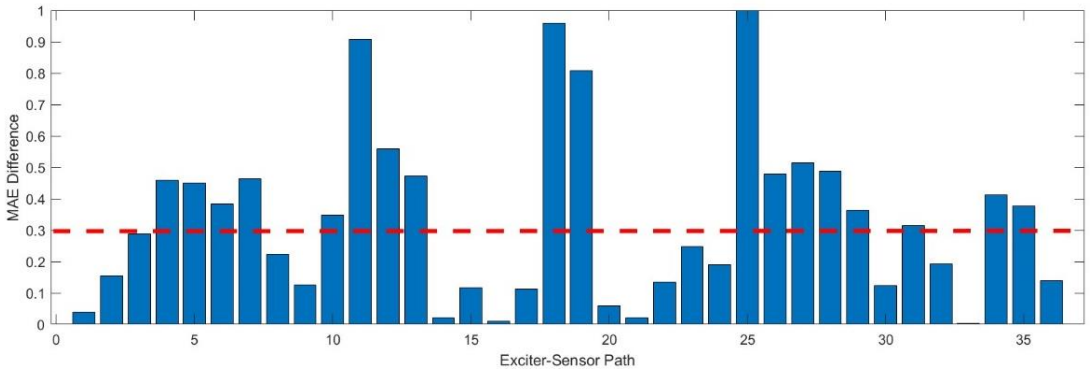

Figure 14. MAE difference vs. Exciter-sensor paths for damage D1.

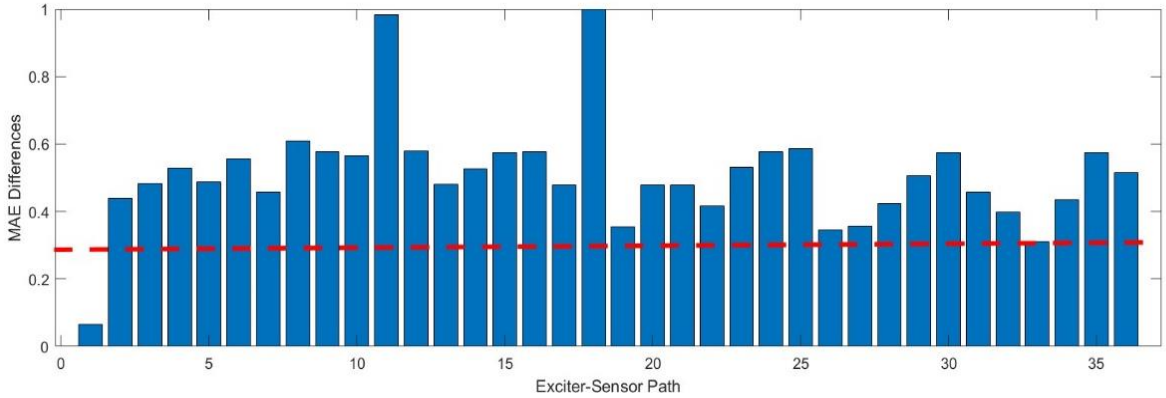

Figure 15. MAE difference vs. Exciter-sensor paths for damage D2.

Table 7. Average MAE for both damage.

Damage ID	Average MAE Difference
D1	0.37
D2	0.48

4.2. Damage Localization

In this section, we apply a reconstruction algorithm to localize the damage on the plate. For this purpose, we only considered those exciter-sensor paths with maximum peak values; hence, these peak values were used as weights for the pixels. We first subtracted the damage signal from the pristine signal and then determined the signal envelope. Here, we exploited time-frequency transformation for this purpose. In this section, we implement a reconstruction algorithm to pinpoint the location of damage on the plate. To facilitate this, we limit our focus to the exciter-sensor paths that display the highest peak values. The first step in this process involves subtracting the pristine, undamaged signal from the damaged signal. Subsequently, we ascertain the signal envelope. We utilize a time-frequency transformation to leverage its capabilities to identify and analyze signal components effectively. In this study, we used smoothed pseudo-Wigner Ville distribution (SPWVD) to obtain the maximum energy distribution curve in time domain. SPWVD possesses two inherent properties; first, it exhibits an anti-noise characteristic, allowing filtered energy to pass through an exceptionally narrow passband. As a result, the impact of low SNR value can be effectively diminished. Secondly, unlike linear Time-Frequency (TF) distributions, which provide only an approximate energy distribution in the TF domain, SPWVD accurately represents the true TF energy distribution of the signal. This precise estimation enables the identification and assessment of damage-related features with high accuracy [29].

$$W(t,\omega)\int z\left(t+\frac{\tau}{2}\right)z^{*}\left(t-\frac{\tau}{2}\right)e^{-i\omega\tau} \tag{10}$$

$$Envelop = max(W(t,\omega)) \tag{11}$$

In addition, we utilized the normal distribution to reduce the width of the generated signal envelope. This technique involves using the maximum peak value of the signal as the mean (average) of the normal distribution. The normal distribution, also known as the Gaussian distribution, is a symmetric probability distribution about the mean. By centering this around the maximum peak value using it as a windowing function, we effectively narrow the envelope's width, focusing more precisely on the region of interest within the signal. This technique provides a more focused and accurate understanding of where potential anomalies, such as damage, might occur within the signal. Figure 16 shows the pristine signal and its comparison with the damage signal D1 for a particular exciter-sensor path.

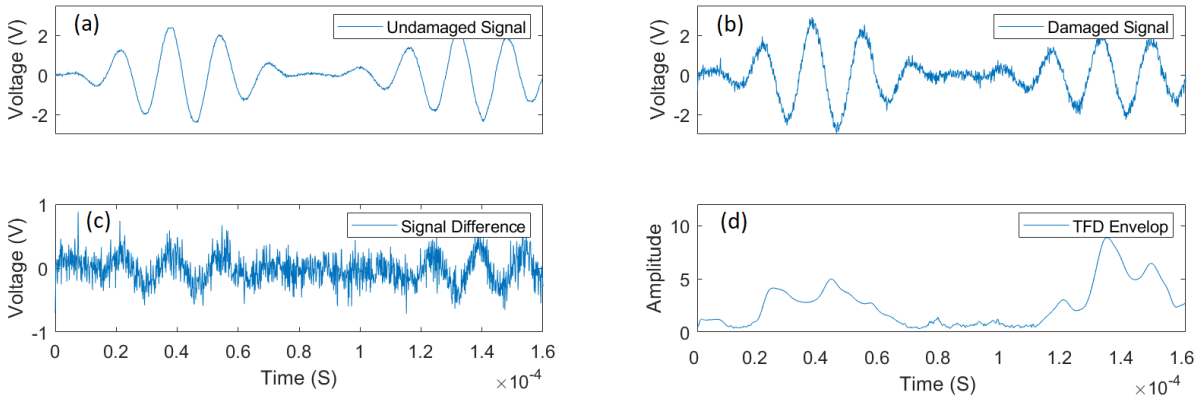

Figure 16. (**a**) is the pristine signal, (**b**) represents the damage signal, (**c**) are the signal differences, (**d**) illustrates the energy envelop obtained by the SPWVD.

The Figures 17 and 18 show the location of the damage D1 and D2, respectively. As we can observe, the position of D1 was determined by utilizing only two exciter-sensor paths, as the proposed autoencoder scheme accurately determined which exciter-sensor paths were optimal for localized damage. However, the result can be made more precise by adding more paths.

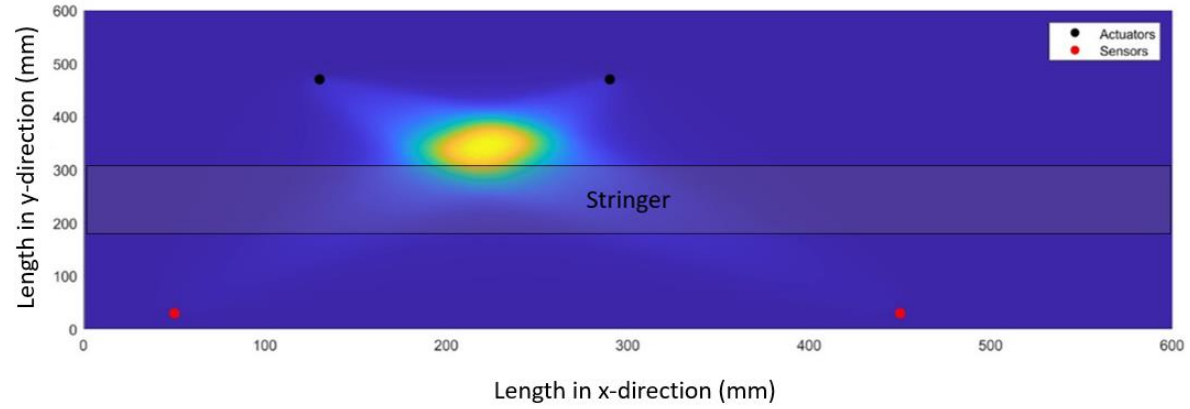

Figure 17. Damage D1 position on the plate.

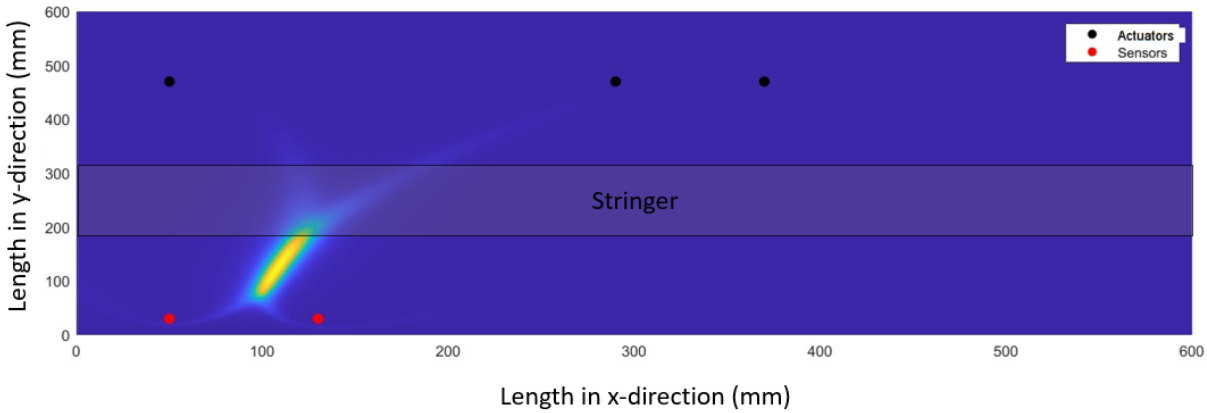

Figure 18. Damage D2 position on the plate.

5. Conclusions

This study used an autoencoder that integrated a bidirectional Long Short-Term Memory (BiLSTM) layer with a Maximal Overlap Discrete Wavelet Transform (MODWT) layer. This configuration aimed to identify anomalies in Lamb wave signals as they propagated

through a composite structure. Our deep learning approach was trained on 720 raw baseline signals, encompassing 36 distinct exciter-sensor paths. This proposed method was validated using unseen datasets comprising 72 randomly selected signals. One of the primary strengths of our approach is its ability to work directly with raw oscilloscope signals, thus eliminating the need for extensive data preparation. To ascertain the effectiveness of our method, we compared the validation accuracy with that of a pure LSTM-based deep model and a 1D Convolutional Neural Network (CNN) model. The results demonstrated that our proposed method performed admirably. To detect anomalies, we introduced damaged signals to the trained encoder model and established threshold values derived from the error generated by the model on the baseline signals. We observed that datasets involving multiple exciter-damage paths exceeded these threshold values, indicating structural damage. Interestingly, paths that passed close to or directly across the damage produced higher error values. This observation proved instrumental in accurately identifying the precise location of the damage within the structure. This approach has the potential to greatly enhance our ability to detect and locate structural damage in composite structures. One limitation of using the proposed scheme is its high sensitivity. MODWT + Bi-LSTM is sensitive to the signal variation which enables models to detect anomalies at an early stage; however, it also increases the chances of detecting false positive results. For such a case, careful model calibration and parameter tunning as well as pre-processing of the input signals are recommended to optimize the model sensitivity and performance.

Author Contributions: S.H.M.R. conducted the primary research work and wrote the manuscript. M.A. provided valuable assistance and supervised the project. S.S.H.Z. contributed resources, technical guidance, and supervision. M.T. offered technical support and assistance. A.M. provided crucial technical support, supervision, and funding for the project. All authors have read and agreed to the published version of the manuscript.

Funding: Major APC was funded by the National University of Science & Technology (NUST).

Institutional Review Board Statement: Not Applicable.

Informed Consent Statement: Not Applicable.

Data Availability Statement: The data presented in this study are available on request from the corresponding author.

Conflicts of Interest: The funders had no role in the design of the study; in the collection, analyses, or interpretation of data; in the writing of the manuscript; or in the decision to publish the results.

References

1. Cho, S.; Yun, C.-B.; Lynch, J.P.; Zimmerman, A.T.; Spencer, B.F., Jr.; Nagayama, T. Smart Wireless Sensor Technology for Structural Health Monitoring of Civil Structures. *Steel Struct.* **2008**, *8*, 267–275.
2. Giurgiutiu, V. *Structural Health Monitoring with Piezoelectric Wafer Active Sensors: With Piezoelectric Wafer Active Sensors*; Elsevier: Amsterdam, The Netherlands, 2007; ISBN 0080556795.
3. Giurgiutiu, V. Lamb Wave Generation with Piezoelectric Wafer Active Sensors for Structural Health Monitoring. In Proceedings of the Smart Structures and Materials 2003: Smart Structures and Integrated Systems; International Society for Optics and Photonics, San Diego, CA, USA, 2–6 March 2002; Volume 5056, pp. 111–123.
4. Ye, X.W.; Jin, T.; Yun, C.B. A Review on Deep Learning-Based Structural Health Monitoring of Civil Infrastructures. *Smart Struct. Syst.* **2019**, *24*, 567–585.
5. Alazzawi, O.; Wang, D. Damage Identification Using the PZT Impedance Signals and Residual Learning Algorithm. *J. Civ. Struct. Health Monit.* **2021**, *11*, 1225–1238. [CrossRef]
6. Wang, X.; Mazumder, R.K.; Salarieh, B.; Salman, A.M.; Shafieezadeh, A.; Li, Y. Machine learning for risk and resilience assessment in structural engineering: Progress and future trends. *J. Struct. Eng.* **2022**, *148*, 3122003.
7. Zhang, Z.; Pan, H.; Wang, X.; Lin, Z. Machine Learning-Enriched Lamb Wave Approaches for Automated Damage Detection. *Sensors* **2020**, *20*, 1790. [CrossRef]
8. Zhang, Z.; Sun, C. Structural Damage Identification via Physics-Guided Machine Learning: A Methodology Integrating Pattern Recognition with Finite Element Model Updating. *Struct. Health Monit.* **2021**, *20*, 1675–1688. [CrossRef]
9. Rai, A.; Mitra, M. Lamb Wave Based Damage Detection in Metallic Plates Using Multi-Headed 1-Dimensional Convolutional Neural Network. *Smart Mater. Struct.* **2021**, *30*, 35010. [CrossRef]

10. Wang, X.; Zhang, X.; Shahzad, M.M. A Novel Structural Damage Identification Scheme Based on Deep Learning Framework. *Structures* **2021**, *29*, 1537–1549. [CrossRef]
11. Xu, L.; Yuan, S.; Chen, J.; Ren, Y. Guided Wave-Convolutional Neural Network Based Fatigue Crack Diagnosis of Aircraft Structures. *Sensors* **2019**, *19*, 3567. [CrossRef]
12. Li, S.; Zuo, X.; Li, Z.; Wang, H. Applying Deep Learning to Continuous Bridge Deflection Detected by Fiber Optic Gyroscope for Damage Detection. *Sensors* **2020**, *20*, 911. [CrossRef]
13. Hung, D.V.; Hung, H.M.; Anh, P.H.; Thang, N.T. Structural Damage Detection Using Hybrid Deep Learning Algorithm. *J. Sci. Technol. Civ. Eng. (STCE)-NUCE* **2020**, *14*, 53–64. [CrossRef]
14. Momeni, H.; Ebrahimkhanlou, A. High-Dimensional Data Analytics in Structural Health Monitoring and Non-Destructive Evaluation: A Review Paper. *Smart Mater. Struct.* **2022**, *31*, 043001.
15. Gao, Y.; Liu, X.; Xiang, J. Fault Detection in Gears Using Fault Samples Enlarged by a Combination of Numerical Simulation and a Generative Adversarial Network. *IEEE/ASME Trans. Mechatron.* **2021**, *27*, 3798–3805. [CrossRef]
16. Taylor, L.; Nitschke, G. Improving Deep Learning with Generic Data Augmentation. In Proceedings of the 2018 IEEE Symposium Series on Computational Intelligence, Bangalore, India, 18–21 November 2018.
17. Oh, C.; Han, S.; Jeong, J. Time-Series Data Augmentation Based on Interpolation. *Procedia Comput. Sci.* **2020**, *175*, 64–71. [CrossRef]
18. Cui, X.; Goel, V.; Kingsbury, B. Data Augmentation for Deep Neural Network Acoustic Modeling. *IEEE/ACM Trans. Audio Speech Lang. Process.* **2015**, *23*, 1469–1477.
19. Li, W.; Chen, C.; Zhang, M.; Li, H.; Du, Q. Data Augmentation for Hyperspectral Image Classification with Deep CNN. *IEEE Geosci. Remote Sens. Lett.* **2019**, *16*, 593–597. [CrossRef]
20. Reconstruct Inputs to Detect Anomalies, Remove Noise, and Generate Images and Text. Available online: https://www.mathworks.com/discovery/autoencoder.html (accessed on 11 June 2023).
21. Torabi, H.; Mirtaheri, S.L.; Greco, S. Practical Autoencoder Based Anomaly Detection by Using Vector Reconstruction Error. *Cybersecurity* **2023**, *6*, 1. [CrossRef]
22. Recurrent Neural Network (RNN). Available online: https://www.mathworks.com/discovery/rnn.html (accessed on 11 June 2023).
23. Said Elsayed, M.; Le-Khac, N.-A.; Dev, S.; Jurcut, A.D. Network Anomaly Detection Using LSTM Based Autoencoder. In Proceedings of the 16th ACM Symposium on QoS and Security for Wireless and Mobile Networks, Alicante, Spain, 16–20 November 2020; pp. 37–45.
24. Lu, Y.; Tang, L.; Chen, C.; Zhou, L.; Liu, Z.; Liu, Y.; Jiang, Z.; Yang, B. Reconstruction of Structural Long-Term Acceleration Response Based on BiLSTM Networks. *Eng. Struct.* **2023**, *285*, 116000. [CrossRef]
25. Li, S.; Li, W.; Cook, C.; Zhu, C.; Gao, Y. Independently Recurrent Neural Network (Indrnn): Building a Longer and Deeper Rnn. In Proceedings of the IEEE Conference on Computer Vision and Pattern Recognition, Salt Lake City, UT, USA, 18–23 June 2018; pp. 5457–5466.
26. Maximal Overlap Discrete Wavelet Transform. Available online: https://www.mathworks.com/help/wavelet/ref/modwt.html (accessed on 11 June 2023).
27. Xiao, F.; Lu, T.; Wu, M.; Ai, Q. Maximal Overlap Discrete Wavelet Transform and Deep Learning for Robust Denoising and Detection of Power Quality Disturbance. *IET Gener. Transm. Distrib.* **2020**, *14*, 140–147. [CrossRef]
28. Moll, J.; Kexel, C.; Kathol, J.; Fritzen, C.-P.; Moix-Bonet, M.; Willberg, C.; Rennoch, M.; Koerdt, M.; Herrmann, A. Guided Waves for Damage Detection in Complex Composite Structures: The Influence of Omega Stringer and Different Reference Damage Size. *Appl. Sci.* **2020**, *10*, 3068.
29. Rizvi, S.H.; Abbas, M. Lamb Wave Damage Severity Estimation Using Ensemble-Based Machine Learning Method with Separate Model Network. *Smart Mater. Struct.* **2021**, *30*, 115016. [CrossRef]